

Possibility and design of resonant terahertz emitters based on nanoscale strained silicon plasma wave transistors with enhanced mobility

This content has been downloaded from IOPscience. Please scroll down to see the full text.

2014 Jpn. J. Appl. Phys. 53 06JE08

(<http://iopscience.iop.org/1347-4065/53/6S/06JE08>)

View [the table of contents for this issue](#), or go to the [journal homepage](#) for more

Download details:

IP Address: 143.248.143.193

This content was downloaded on 14/03/2016 at 06:18

Please note that [terms and conditions apply](#).

Possibility and design of resonant terahertz emitters based on nanoscale strained silicon plasma wave transistors with enhanced mobility

Jong Yul Park¹, Sung-Ho Kim¹, Yang-Kyu Choi², Songcheol Hong², Sang-Gug Lee², and Kyung Rok Kim^{1*}

¹School of Electrical and Computer Engineering, Ulsan National Institute of Science and Technology, Ulsan 689-798, Republic of Korea

²Department of Electrical Engineering, Korea Advanced Institute of Science and Technology, Daejeon 305-701, Republic of Korea

E-mail: krkim@unist.ac.kr

Received December 2, 2013; accepted February 10, 2014; published online May 15, 2014

In this paper, we report the possibility of silicon (Si) plasma wave transistor (PWT) as a resonant terahertz (THz) emitter based on the theoretical analysis focusing on the strained Si with enhanced mobility. Under asymmetric boundary conditions for plasma wave instability, the amplitude of plasma wave in FET channel increases and this plasma wave increment provides the basis of the electromagnetic (EM) wave emission from FET. Because this instability is controlled by manipulation of plasma wave velocity (s) and electron drift velocity (v_0), we propose the design window based on $s-v_0$ plot which determines whether the device operates as the resonant THz emitters considering all the required physical conditions. It is expected from the proposed design window that strained Si PWT down to 10 nm gate length with enhanced channel mobility of $500 \text{ cm}^2 \cdot \text{V}^{-1} \cdot \text{s}^{-1}$ can operate as a resonant emitter in THz frequency range. © 2014 The Japan Society of Applied Physics

1. Introduction

Terahertz (THz) technology, which is mainly composed of imaging,¹⁻³ spectroscopy,⁴⁻⁶ and communication,^{7,8} is appealing to researchers due to its useful properties and various applications such as food inspection^{9,10} and security.¹¹⁻¹³ Among the electronic device-based THz wave emitter^{14,15} and detector,¹⁶⁻¹⁸ plasma wave transistor (PWT) based on silicon (Si) FET structure has advantages in terms of low cost and large scale integration.^{19,20} After the theoretical concept of PWT has been proposed by Dyakonov and Shur,²¹ while PWT THz detectors are actively developed^{22,23} and it has been expected that a high electron mobility transistor (HEMT) operates as a THz emitters,²⁴⁻²⁶ there has been no significant investigation for the possibility of THz emitters based on Si PWT due to its relatively low mobility. As the gate length of nano-CMOS has been scaled down to nanoscale regime around 10 nm, however, the extremely scaled channel length can compensate the loss from low channel mobility in Si FETs. In addition, the mobility of Si FET can be improved by the strained Si technology.^{27,28}

Therefore, we set the aim of this work to illustrate that it is feasible to make THz emitter based on strained Si FET with nanoscale channel length. In order to investigate this feasibility in the analytical way, we proposed the design window based on the physical conditions for PWT to be operated as THz emitter. The physical background is provided to explain hydrodynamic behavior in the channel of FET for plasma wave instability. The proposed design window for THz emission is firstly implemented with typical device parameters assuming arbitrary semiconducting materials and then, the possibility of resonant THz emitter in Si technology is discussed by taking the practical examples of GaAs and strained Si as channel material.

2. Physical background

In order to understand plasma wave properties on shallow water analogy,²¹ it is important to describe two-dimensional electron gas (2DEG) behavior which is governed by the following hydrodynamic Euler Eq. (1) and continuity Eq. (2):

$$\left(\frac{\partial}{\partial t} + v \frac{\partial}{\partial x} \right) m v = -e \frac{\partial U}{\partial x} - \frac{m v}{\tau_p}, \quad (1)$$

$$\frac{\partial U}{\partial t} + \frac{\partial(Uv)}{\partial x} = 0, \quad (2)$$

where v is local electron velocity, $U(x, t)$ is voltage difference between a gate and a channel, m is the effective mass of electron, e is the elementary electronic charge, and τ_p is the momentum relaxation time. Figure 1 illustrates the spatial distribution of the channel plasma waves between source ($x = 0$) and drain ($x = L$) with schematic squares and its intensity which represents 2DEG density modulations. When the gate overdrive voltage $U_0 = U_g - U_{th} > 0$ where U_{th} is the threshold voltage of FET and U_g is dc gate voltage, and the drain-to-source voltage $U_{DS} = 0$, the plasma wave by channel 2DEG is generated with its velocity $s = (eU_0/m)^{1/2}$ [Fig. 1(a)]. In this case of $v_0 = 0$ from $U_{DS} = 0$, the plasma wave has a dispersion relation $k = \pm\omega/s$, where ω is the plasma wave frequency. As $U_{DS} > 0$, the electrons move with the drift velocity v_0 and the plasma wave, which is now carried along by the current flux, moves with $s_1 = v_0 + s$ for downstream and $s_2 = v_0 - s$ for upstream. It means that the dispersion relation changes to $k_+ = \omega/(v_0 + s)$ for downstream and $k_- = \omega/(v_0 - s)$ for upstream. In this case, since the solutions of $v = v_0 + v_1 e^{-i\omega t}$ and $U = U_0 + U_1 e^{-i\omega t}$ from Eqs. (1) and (2) have temporal ($e^{-i\omega t}$) and spatial perturbations (v_1, U_1) through the channel, channel 2DEG density n can be expressed by the relation of $n = CU/e$ with gate-to-channel areal capacitance (C) as

$$n = n_0 + n_1 e^{-i\omega t}, \quad (3)$$

$$n_1 = C_+ e^{ik_+ x} + C_- e^{ik_- x}, \quad (4)$$

where $n_0 = CU_0/e$, n_1 is spatial perturbation of n , C_+ and C_- are perturbation coefficients for downstream and upstream, respectively. The difference of the speed between upstream and downstream is the reason for the plasma wave amplification due to reflection coefficient at drain side. The reflection coefficient at source side $C_-/C_+ = R_s = -1$ is obtained by Eqs. (3) and (4) with boundary condition $U(x = 0) = U_0$, which is DC gate overdrive voltage at source side (AC short). With this result, the reflection coefficient at drain side R_d is yielded by modulating the first order

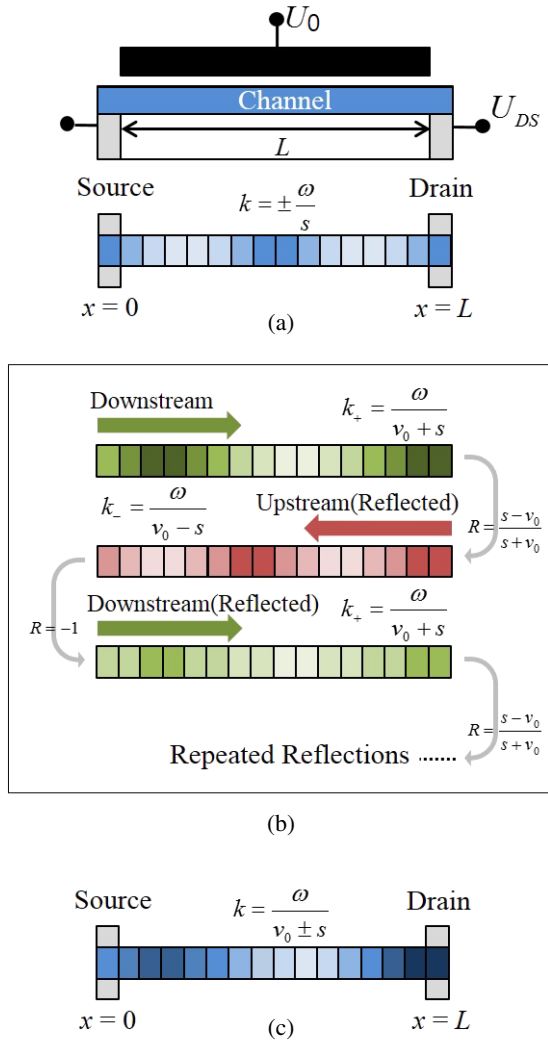


Fig. 1. (Color online) Top view of PWT channel, (a) when $U > 0$ and $U_{DS} = 0$ with schematic structure. (b) Three wave components when $U > 0$ and $U_{DS} > 0$. (c) Top view of PWT channel when $U > 0$ and $U_{DS} > 0$.

continuity equation considering n and v , which results in the first order current flux $j_1(x)$ as

$$j_1(x) = \frac{\omega}{k_+} C_+ e^{ik_+x} + \frac{\omega}{k_-} C_- e^{ik_-x}. \quad (5)$$

Therefore, from the boundary condition $j_1(x=L) = 0$ at drain (AC open), $R_d = (C_- k_+) / (C_+ k_-) = (s - v_0) / (s + v_0) < 1$. The downstream from source side changes to upstream at drain side by the reflection with decreased amplitude ($R_d < 1$) as well as larger wave number. Subsequently, it is reflected at source side only with 180° phase difference by $R_s = -1$ [Fig. 1(b)]. We can represent the plasma wave growth with oscillation from the superposition of all wave components as shown in Fig. 1(c). The plasma wave frequency ω is obtained by linearizing Eqs. (1) and (2) with the perturbations of v , U , and n as $\omega = \omega' + i\omega''$:

$$\omega' = \frac{|s^2 - v_0^2|}{2Ls} N\pi, \quad (6)$$

$$\omega'' = \frac{s^2 - v_0^2}{2Ls} \ln \left| \frac{s + v_0}{s - v_0} \right| - \frac{1}{2\tau_p}, \quad (7)$$

where L is the channel length and N is an odd integer. This theoretical solution indicates that the plasma wave increment

($\omega'' > 0$) can be observed even if the channel is not in a ballistic regime with finite mobility and momentum relaxation time $\tau_p = \mu m / e$ where μ is channel mobility. In this paper, we assume $\tau_p = 100$ fs ($\mu \cong 2000 \text{ cm}^2 \cdot \text{V}^{-1} \cdot \text{s}^{-1}$, $m \cong 0.09m_0$) for the typical case. Also, for practical examples, we choose $\tau_p = 160$ fs ($\mu \cong 4500 \text{ cm}^2 \cdot \text{V}^{-1} \cdot \text{s}^{-1}$,²⁹ $m \cong 0.063m_0$) for GaAs case and $\tau_p = 50$ fs ($\mu \cong 500 \text{ cm}^2 \cdot \text{V}^{-1} \cdot \text{s}^{-1}$,²⁸ $m \cong 0.19m_0$) for strained Si case.

The effects of the finite τ_p on the wave increment have been investigated in Fig. 2(a), which shows the plot of plasma wave increment ω'' as the function of v_0 for a PWT with $L = 50$ nm and $s = 1 \times 10^8$ cm/s for each $\tau_p = 100$ fs, 200 fs, and infinite value (ballistic channel). For $\tau_p = \infty$ (dashed line in Fig. 2), it is shown that the wave increment can occur even for very small $v_0 \ll s$ ($s_1 \cong s_2$). When τ_p becomes finite and decreases [lines in Fig. 2(a)], however, there is a finite range of v_0 to be $\omega'' > 0$ due to the loss term of $-1/(2\tau_p)$ as expected from Eq. (7). The reason why ω'' shows non-monotonic behavior as a function of v_0 can be explained by the plot of each natural logarithm and its pre-factor term as shown in Fig. 2(b). Firstly from a natural logarithm term of $\ln|(s + v_0)/(s - v_0)|$ in Eq. (7), the increase of v_0 results in enhancing ω'' since $s + v_0$ becomes much larger than $s - v_0$. As exceeding certain value of v_0 , however, ω'' starts to decrease because it takes long round-trip time (τ) of the plasma wave between source and drain as given by²¹⁾

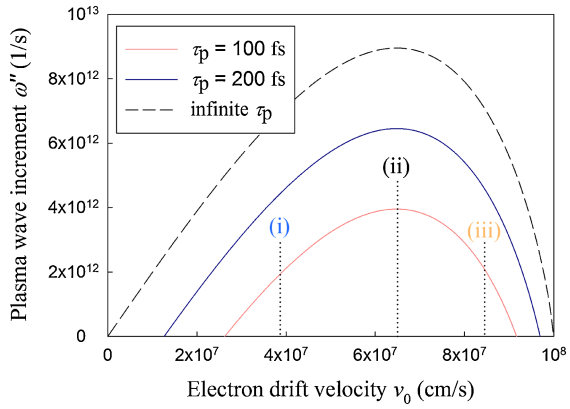
$$\tau = \frac{L}{s + v_0} + \frac{L}{s - v_0} = \frac{2Ls}{s^2 - v_0^2}, \quad (8)$$

which corresponds to a pre-factor of log term in Eq. (7). Therefore, as shown in Fig. 2(c), we confirmed that the higher ω'' means the faster plasma wave grows in a shorter elapsed time by comparing each plasma wave oscillation which corresponds to the points of (i), (ii), and (iii) as noted in Fig. 2(a). In cases of (i) and (iii) with the same ω'' , it is also shown that there is only frequency difference between (i) (smaller v_0) and (iii) (larger v_0) while keeping amplitude growth same at a certain elapsed time.

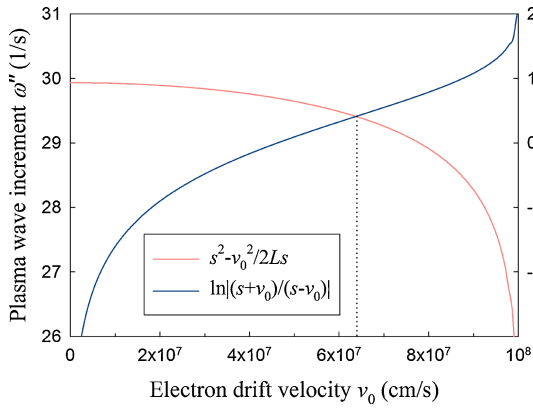
To investigate the effects of the other important design parameter s on ω'' , the plot of ω'' as a function of s has been provided with fixed $v_0 = 3 \times 10^7$ cm/s in Fig. 3, which indicates that there is the saturation of ω'' when s increases much larger than v_0 . If we increases s until $v_0 \ll s$, Eq. (7) converges to the inverse electron transit time $\omega'' = v_0/L$, which means that no matter how we increase s in order to make the amplitude grow faster, there is a limitation by electron transit time L/v_0 because plasma wave propagates by electrons.

3. Results and discussion

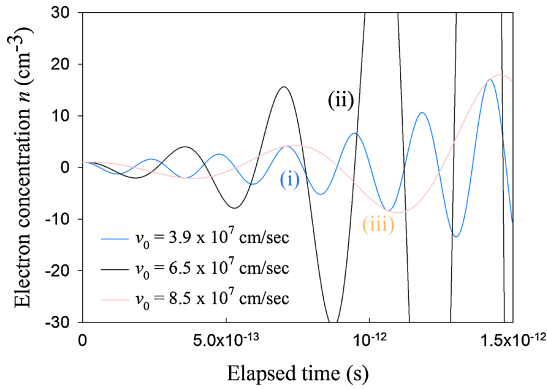
Based on the theoretical analysis in Sect. 2, we propose the design window for making PWT THz emitter by drawing $s-v_0$ plot first because s and v_0 are independently controlled by U and U_{DS} , respectively. Then, how plasma wave grows can be described by ω'' on $s-v_0$ plot. To do this, we present Figs. 4(a) and 4(b) illustrate ω'' as a function of v_0 and s for the fixed s and v_0 , respectively, for the PWT emitter with $L = 50$ nm and $\tau_p = 100$ fs as typical device parameters assuming arbitrary semiconducting materials. By assigning ω'' as z -axis on $s-v_0$ plot, the operation regime of PWT



(a)



(b)



(c)

Fig. 2. (Color online) (a) $\omega''-v_0$ plot for $\tau_p = 100, 200,$ and ∞ fs. (b) $\omega''-v_0/s$ plot with natural log scale. (c) Temporal variation of electron concentration for $v_0 = 2.6 \times 10^7, 3.9 \times 10^7, 6.5 \times 10^7,$ and 8.5×10^7 cm/s.

emitter can be presented as 3D plot as shown in Fig. 5. Basically, this 3D plot is generally applicable for various materials with their own physical parameters but, the PWT THz emitter operation is limited by the required physical conditions, which are summarized in Table I with parameters of $\omega, \tau_p, s,$ and v_0 . The physically reasonable design window would be more reduced due to the limitations of each condition in Table I. Especially, the operation regime is strongly confined by the physical condition related with v_0 because v_0 cannot exceed the injection velocity $v_{inj} = (2k_B T / \pi m)^{1/2}$, where k_B is the Boltzmann constant, and T is temperature.

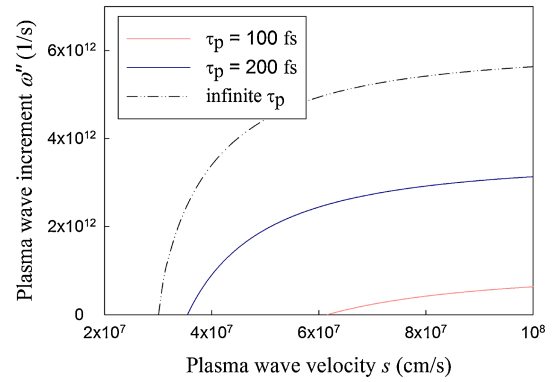
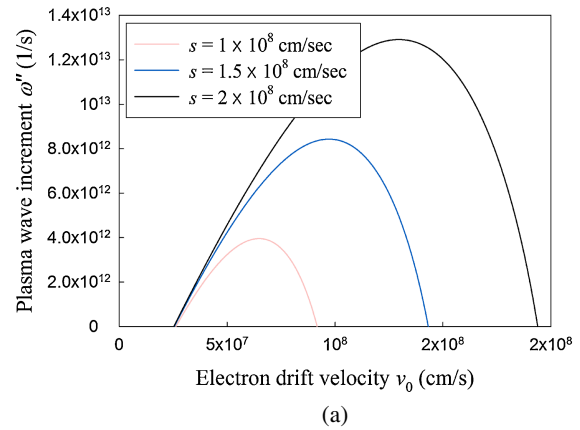
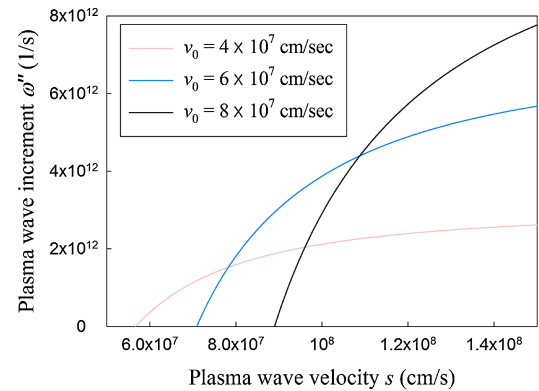


Fig. 3. (Color online) $\omega''-s$ plot which shows wave increment saturation.



(a)



(b)

Fig. 4. (Color online) (a) $\omega''-v_0$ plot for $s = 1 \times 10^8, 1.5 \times 10^8,$ and 2×10^8 cm/s. (b) $\omega''-s$ plot for $v = 4 \times 10^7, 6 \times 10^7,$ and 8×10^7 cm/s.

Table I. Physical conditions for making THz emitters.

Physical condition	Criteria
Underdamped	$\omega\tau_p > 1$
Instability	$v_0 < v_{inj} < s$
Increment	$\omega'' > 0$
Frequency	$f < 10$ THz

Figure 6(a) shows the finally confined design window as 2D plot which designates emission window for the PWT with $L = 50$ nm, $v_{inj} = 3 \times 10^7$ cm/s and $\tau_p = 100$ fs. Using Eqs. (6), (7), and the conditions in Table I, the boundaries of design window are determined by the following equations:

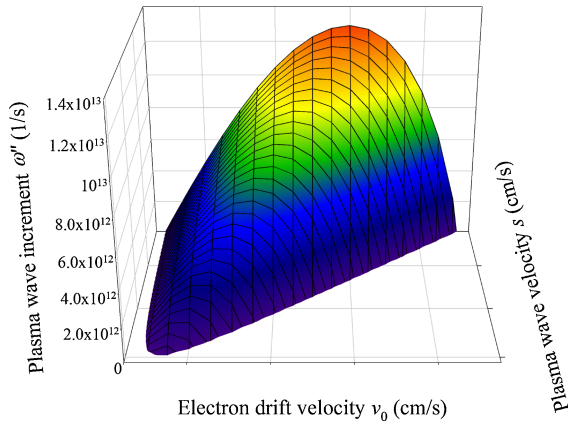


Fig. 5. (Color online) s - v_0 - ω'' plot. Even if it shows broad v_0 and high ω'' range, we only use limited range due to physical conditions.

$$s = \left(\tau_p |1 - M^2| \ln \left| \frac{1 + M}{1 - M} \right| \right)^{-1} L, \quad (9)$$

$$s = (1 \times 10^{13}) \frac{4L}{|1 - M^2|}, \quad (10)$$

$$s = \frac{4L}{2\pi\tau_p |1 - M^2|}, \quad (11)$$

where $M = v_0/s$ is the mach number. Equation (9) is derived from Eq. (7) with $\omega'' = 0$ and the physical condition $\omega'' > 0$ can be represented with the contour lines in Fig. 5. The criterion of maximum frequency (10 THz) leads to Eq. (10) and indicates what frequency the plasma wave have at a certain point in the emission window. Even if the physical condition $\omega\tau_p > 1$, which results in Eq. (11), does not affect on the design window in Fig. 6(a), it becomes dominant as scaling down channel length. From the contour lines in the emission area, it is shown that the maximum ω'' is located at $v_0 = v_{inj}$ with highest s . Figure 6(b) describes the extension of the design window if the momentum relaxation time increases from 100 to 200 fs. It is remarkable that the confined v_0 range can be extended drastically according to the increase of τ_p . In the other design case with varying L for fixed $\tau_p = 100$ fs, as shown in Fig. 6(c), the shapes of the design window changes with keeping the minimum M (M_{min}) which is yielded by calculating an intersection point from Eqs. (9) and (10):

$$M_{min} = \frac{\exp(4\tau_p \times 10^{13})^{-1} - 1}{\exp(4\tau_p \times 10^{13})^{-1} + 1}. \quad (12)$$

It means that the intersection between the line of M_{min} and $v_0 = v_{inj}$ let us know the maximum L (L_{max}) which can be expressed by the following equation:

$$L_{max} = \frac{s_{max} |1 - M_{min}^2|}{4 \times 10^{13}}, \quad (13)$$

where $s_{max} = v_{inj}/M_{min}$. In this typical case, L_{max} is about 60 nm. Moreover, it can be noted that the range of v_0 is extended to the lower value and 10 THz is achievable for relatively low s as scaling down the gate length.

Considering this L_{max} for the various channel materials in PWTs, the realistic examples of PWT design window for THz emitter can be drawn with their own material properties as shown in Figs. 7 and 8. Figure 7 shows the design

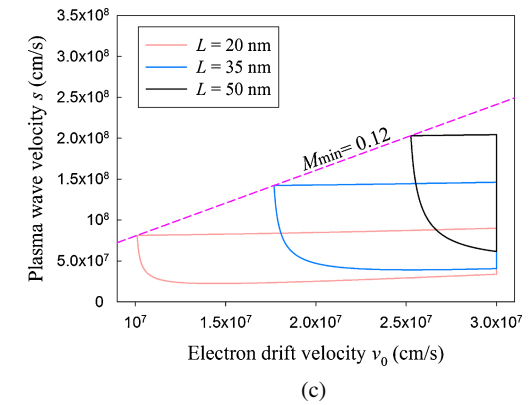
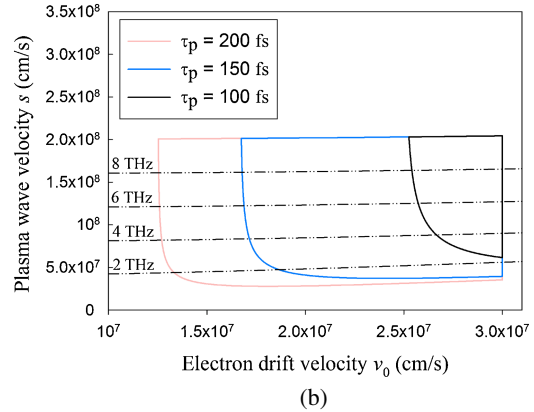
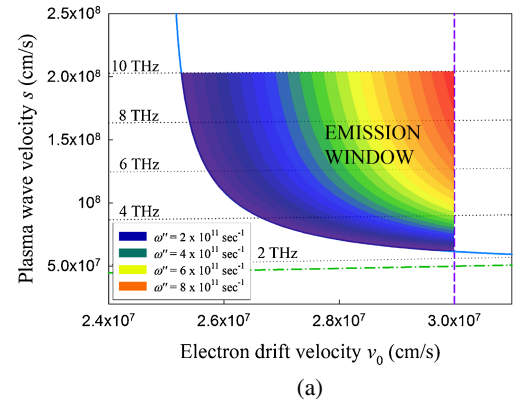


Fig. 6. (Color online) Emission window for the general case. (a) Emission window with contour line meaning wave increment ω'' . The underdamped (dash-dot line), instability (dashed line), increment (solid line), frequency (dotted line) conditions are respectively used to plot the design window. (b) Emission window for THz emitter with fixed gate length $L = 50$ nm. Each area shares similar frequency at same plasma wave velocity. (c) Emission window for THz emitter with fixed momentum relaxation time. Each area has totally different frequency at same plasma wave velocity.

window for the example of GaAs with $L = 50$ nm (cf. $L_{max,GaAs} = 58$ nm), $v_{inj} = 2 \times 10^7$ cm/s and $\tau_p = 160$ fs from $m = 0.063m_0$ and $\mu = 4500$ cm²·V⁻¹·s⁻¹.²⁹) The emission window for GaAs-based PWT is determined with $1.57 \times 10^7 < v_0 < v_{inj} = 2 \times 10^7$ cm/s and $3.6 \times 10^7 < s < 2 \times 10^8$ cm/s in the operation frequency range of $1.5 < f = \omega/2\pi < 10$ THz. In Si technology, the conventional Si FETs exhibit generally the channel mobility of $\mu = 250$ cm²·V⁻¹·s⁻¹,³⁰) which leads to the extremely small design window by $L_{max,Si} = 7$ nm. If we consider strained Si technology with enhanced channel mobility $\mu = 500$ cm²·V⁻¹·s⁻¹,²⁸) however, L_{max} has been nearly doubled

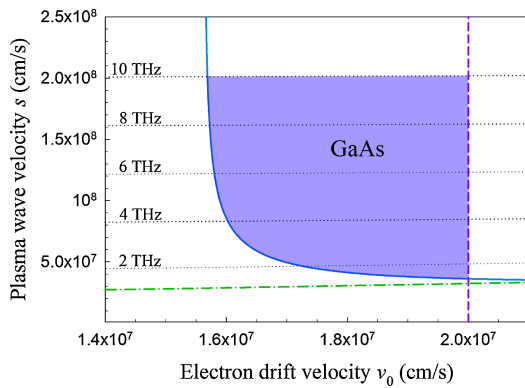


Fig. 7. (Color online) Emission window for GaAs case with $L = 50$ nm. The underdamped (dash-dot line), instability (dashed line), increment (solid line), frequency (dotted line) conditions are respectively used to plot the design window.

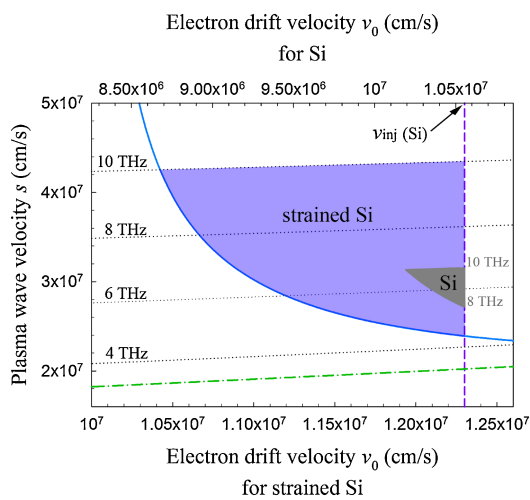


Fig. 8. (Color online) Emission windows for strained Si case with $L = 10$ nm and Si case with $L_{\max, \text{Si}} = 7$ nm. The shape is similar to the GaAs and general case. The underdamped (dash-dot line), instability (dashed line), increment (solid line), frequency (dotted line) conditions are respectively used to plot the design window.

from the conventional Si technology as $L_{\max, \text{Si}} = 12$ nm with $v_{\text{inj}} = 1.23 \times 10^7$ cm/s and $\tau_p = 50$ fs by assuming $m = 0.19m_0$ for strained Si. Figure 8 illustrates that the design window for the strained Si with $L = 10$ nm (cf. $L_{\max, \text{Si}} = 12$ nm) can be extended with $1.04 \times 10^7 < v_0 < v_{\text{inj}} = 1.23 \times 10^7$ cm/s and $2.4 \times 10^7 < s < 4.4 \times 10^8$ cm/s in the operation frequency range of $4.5 < f = \omega/2\pi < 10$ THz, which are comparable with compound semiconductor such as GaAs in Fig. 7. By using strained Si with enhanced channel mobility, we found the possibility of resonant THz emitter based on strained Si PWTs by increasing L_{\max} around 10 nm technology generation.

4. Conclusions

In summary, we have shown that it is possible to design resonant THz emitters based on strained Si PWTs with enhanced mobility. In order to evaluate the operation regime of PWT as resonant THz emitter, we have proposed the design window in the analytical way by investigating the

fundamental physics of plasma wave behaviors in PWTs. The proposed design methodology can be practically applied to create the specific design windows for various resonant PWT emitters based on the required physical conditions and boundary conditions.

Acknowledgements

This research was supported by the Pioneer Research Center Program through the National Research Foundation of Korea funded by the Ministry of Science, ICT & Future Planning (Grant No. 2012-0009594). We the authors are really thankful for helpful discussion with Professor Jae-Hyung Jang and Professor Sung-Min Hong at GIST, Korea.

- 1) S. Ariyoshi, C. Otani, A. Dobroui, H. Matuso, H. Sato, T. Taino, K. Kawase, and H. M. Shimizu, *Jpn. J. Appl. Phys.* **45**, L1004 (2006).
- 2) R. Inoue, N. Uchida, and M. Tonouchi, *Jpn. J. Appl. Phys.* **45**, L824 (2006).
- 3) W. L. Chan, J. Deibel, and D. M. Mittleman, *Rep. Prog. Phys.* **70**, 1325 (2007).
- 4) B. M. Fischer, M. Walther, and P. U. Jepsen, *Phys. Med. Biol.* **47**, 3807 (2002).
- 5) M. V. Tsurkan, N. S. Balbekin, E. A. Sobakinskaya, A. N. Panin, and V. L. Vaks, *Opt. Spectrosc.* **114**, 894 (2013).
- 6) P. A. George, J. Strait, J. Dawlaty, S. Shivaraman, M. Chandrashekar, F. Rana, and M. G. Spencer, *Nano Lett.* **8**, 4248 (2008).
- 7) H.-J. Song and T. Nagatsuma, *IEEE Trans. Terahertz Sci. Technol.* **1**, 256 (2011).
- 8) T. Kleine-Ostmann and T. Nagatsuma, *J. Infrared Millimeter Terahertz Waves* **32**, 143 (2011).
- 9) Z. Yan, Y. Ying, H. Zhang, and H. Yu, *Proc. SPIE* **6373**, 63730R (2006).
- 10) N. Karpowicz, H. Zhong, C. Zhang, K.-I. Lin, J.-S. Hwang, J. Xu, and X.-C. Zhang, *Appl. Phys. Lett.* **86**, 054105 (2005).
- 11) W. R. Tribe, D. A. Newnham, P. F. Taday, and M. C. Kemp, *Proc. SPIE* **5354**, 168 (2004).
- 12) H.-B. Liu, H. Zhong, N. Karpowicz, Y. Chen, and X.-C. Zhang, *Proc. IEEE* **95**, 1514 (2007).
- 13) M. C. Kemp, P. F. Taday, B. E. Cole, J. A. Cluff, A. J. Fitzgerald, and W. R. Tribe, *Proc. SPIE* **5070**, 44 (2003).
- 14) I. Morohashi, K. Komori, T. Hidaka, X. L. Wang, M. Ogura, and M. Watanabe, *Jpn. J. Appl. Phys.* **43**, 2125 (2004).
- 15) T. Hattori, S. Arai, and K. Tukamoto, *Jpn. J. Appl. Phys.* **43**, 7546 (2004).
- 16) Z. Piao, M. Tani, and K. Sakai, *Jpn. J. Appl. Phys.* **39**, 96 (2000).
- 17) V. Ryzhii and M. S. Shur, *Jpn. J. Appl. Phys.* **45**, L1118 (2006).
- 18) T. Hattori, K. Egawa, S. Ookuma, and T. Itatani, *Jpn. J. Appl. Phys.* **45**, L422 (2006).
- 19) Y. Deng and M. S. Shur, *Solid-State Electron.* **47**, 1559 (2003).
- 20) W. Knap, M. Dyakonov, D. Coquillat, F. Teppe, N. Dyakonova, J. Łusakowski, K. Karpierz, M. Sakowicz, G. Valusis, D. Seliuta, I. Kasalynas, A. E. Fatimy, Y. M. Meziani, and T. Otsuji, *J. Infrared Millimeter Terahertz Waves* **30**, 1319 (2009).
- 21) M. Dyakonov and M. Shur, *Phys. Rev. Lett.* **71**, 2465 (1993).
- 22) M. Dyakonov and M. Shur, *IEEE Trans. Electron Devices* **43**, 380 (1996).
- 23) W. Knap, N. V. Dyakonova, F. Schuster, D. Coquillat, F. Teppe, B. Giffard, D. B. But, O. G. Golenkov, F. F. Sizov, T. Watanabe, Y. Tanimoto, and T. Otsuji, *Proc. SPIE* **8496**, 84960I (2012).
- 24) M. I. Dyakonov and M. S. Shur, *IEEE Trans. Electron Devices* **43**, 1640 (1996).
- 25) V. Ryzhii, A. Satou, W. Knap, and M. S. Shur, *J. Appl. Phys.* **99**, 084507 (2006).
- 26) T. Onishi, T. Tanigawa, and S. Takigawa, *Appl. Phys. Lett.* **97**, 092117 (2010).
- 27) M. L. Lee, E. A. Fitzgerald, M. T. Bulsara, M. T. Currie, and A. Lochtefeld, *J. Appl. Phys.* **97**, 011101 (2005).
- 28) W. Xiong, C. R. Cleavelin, P. Kohli, C. Huffman, T. Schulz, K. Schrufer, G. Gebara, K. Mathews, P. Patruno, Y. M. L. Vaillant, I. Cayrefourcq, M. Kennard, K. Shin, and T. J. K. Liu, *IEEE Electron Device Lett.* **27**, 612 (2006).
- 29) K. Rajagopalan and R. Droopad, *IEEE Electron Device Lett.* **27**, 959 (2006).
- 30) S. Takagi, A. Toriumi, M. Iwase, and H. Tango, *IEEE Trans. Electron Devices* **41**, 2363 (1994).